Oceanologia (2017) 59, 350—364

Available online at www.sciencedirect.com

ScienceDirect

journal homepage: www.journals.elsevier.com/oceanologia/

ORIGINAL RESEARCH ARTICLE

# Modelling nearshore hydrodynamics and circulation under the impact of high waves at the coast of Varkiza in Saronic-Athens Gulf

**Kostas A. Belibassakis** *, **Flora E. Karathanasi**

*School of Naval Architecture & Marine Engineering, National Technical University of Athens, Athens, Greece*

Received 18 January 2017; accepted 2 April 2017
Available online 19 April 2017

**KEYWORDS**
High waves;
Wave/current modelling;
Sediment transport;
Varkiza coast

**Summary** A plethora of physical parameters, such as hydro-, litho- and morpho-dynamic characteristics, are essential for understanding the response of coastal systems to intense sea states in terms of sediment transport and shoreline evolution. Nowadays, numerical models are extensively applied to meet the above needs and support coastal planning and management. In the present work, a 2DH dynamic modelling system is used for simulating the hydrodynamic and meteorological/oceanographic characteristics of the Saronic Gulf, in order to examine circulation patterns and predict sediment transport phenomena under high wave conditions at the coast of Varkiza, a sandy beach in the southern Attica, Greece. Time series of wind and wave data were used as input at the open boundaries of the model domain while the model was calibrated and validated through (linear and directional) statistical measures with respect to *in situ* wave measurements, since there was lack of hydrodynamic data at the site of interest.The simulation period of the model was between January 3 and February 19, 2013, with consecutive high waves in-between. The good agreement of the numerical results from the wave and hydrodynamic model with *in situ* measurements confirmed the suitability of the model for the support of sediment transport rates at Varkiza coastal segment. Model results reveal that there is a counter-clockwise water circulation during high waves that contribute to the erosion of the examined beach, which is also confirmed by independent field measurements.
© 2017 The Authors. Production and hosting by Elsevier Sp. z o.o. on behalf of Institute of Oceanology of the Polish Academy of Sciences. This is an open access article under the CC BY-NC-ND license (http://creativecommons.org/licenses/by-nc-nd/4.0/).

* Corresponding author at: School of Naval Architecture & Marine Engineering, National Technical University of Athens, Zografos 15773, Athens, Greece. Tel.: +30 210 7721138; fax: +30 210 7721397.
*E-mail address:* kbel@fluid.mech.ntua.gr (K.A. Belibassakis).
Peer review under the responsibility of Institute of Oceanology of the Polish Academy of Sciences.

ELSEVIER | Production and hosting by Elsevier

http://dx.doi.org/10.1016/j.oceano.2017.04.001
0078-3234/© 2017 The Authors. Production and hosting by Elsevier Sp. z o.o. on behalf of Institute of Oceanology of the Polish Academy of Sciences. This is an open access article under the CC BY-NC-ND license (http://creativecommons.org/licenses/by-nc-nd/4.0/).

## 1. Introduction

Coastal zones receive a wide range of environmental pressures coming either from natural processes (e.g. sea-level rise, storm surges, hurricanes, etc.) or anthropogenic activities (e.g. fisheries, oil and gas extraction, harbour facilities, tourism, etc.). Adding the increasingly disproportional rates of coastal population density compared to the inland (Neumann et al., 2015), there is an imperative need to manage and protect such areas, as well as human life, effectively. Among the measures that should be taken into account is the forecast of coastal morphological changes that are mainly driven by sediment transport gradients.

The essential properties of coastal morphodynamic processes are the interaction between bathymetry/topography and fluid dynamics (Cowell and Thom, 1994; Dodd et al., 2003) that, on the other hand, are responsible to a great extent for the volume displacement during sediment transport. However, morphological changes depend on the evolutionary nature of all the involved complex processes. Sufficient knowledge of coastal geomorphology, wind and wave climate, and the corresponding complex interaction with sediment particles, and better understanding of all the underlying coastal dynamics in various spatio-temporal scales render coastal evolution more predictable.

A wide research field for the representation of coastal dynamics is based on numerical modelling, apart from physical model tests. In a relatively short time and at a low cost, different parameters and scenarios can be applied and tested in the context of an engineering problem but the inherent complexity of the abovementioned dynamic processes renders the development of reliable models a rather demanding task. A lot of research has been carried out in order to develop reliable coupling models, nesting techniques and modelling systems that can scale down the forcing from a large scale (e.g. oceanic waters) to a local one (e.g. coastal waters) so as to predict as accurate as possible sediment transport rates and morphological evolution in coastal areas. Moreover, the understanding of such dynamic mechanisms is crucial not only for the human-oriented activities in the coastal environment and the stability of the coastal/marine structures but also for the quality of the water by transferring pollutants (e.g. Gong et al., 2011) and ecosystem sustainability of nearshore areas, since sediment contributes to the supply and distribution of nutrients and organic materials (e.g. Ikeda et al., 2009).

According to Hanson et al. (2003), coastal morphodynamic models can be divided into six classes: (i) conceptual models (Masselink and Short, 1993; Ruessink and Terwindt, 2000; Weitz and Demlie, 2014); (ii) shoreline evolution models (Jara et al., 2015; Samaras and Koutitas, 2014); (iii) beach profile evolution models (Bernabeu et al., 2003; Karunarathna et al., 2012; Requejo et al., 2008); (iv) 2D horizontal (2DH) morphological models (Dibajnia et al., 2004; El Kadi Abderrezzak et al., 2016; Larroudé, 2008; Nam et al., 2009); (v) quasi-3D (Q3D) morphological models (Chen et al., 2014; Li et al., 2007); and (vi) 3D morphological models (Bai et al., 2003; Lesser et al., 2004; Mayerle et al., 2015; Shengcheng et al., 2014). Specifically, for sediment transport models, there is an extensive review article by Papanicolaou et al. (2008) describing the capabilities, strengths and limitations of numerous computational models while in Van Rijn et al. (2013) advances in sediment transport processes in the coastal environment and future research needs are discussed in detail.

Among the marine dynamic processes, the significance of wind-generated waves stands out mainly due to their structuring nature on the coastal environment in terms of morphological formation and composition. For instance, high-energy ocean events influence among others erosion-accretion dynamics by affecting the sediment transport rates of a beach; the degree of severity from the impacts of such an event at a beach depends not only on the characteristics of the event *per se* but also on the characteristics of the beach and the sensitivity of the surrounding ecosystems. Based on the perspective of the frequency and magnitude of waves, two common modelling approaches for the consideration of wave action in sediment transport modelling that can be implemented are the following: the first one deals with the action of individual high waves that collide with the shore for a short time window (e.g. several hours), and the second one takes into consideration the accumulative action of waves throughout a typical year, with high-energy waves during winter and low-energy waves during summer; see, e.g. Ferreira (2005), Callaghan et al. (2009), Karunarathna et al. (2014), Coco et al. (2014).

The main motivation of this paper is to study the effects of the former case (i.e. high waves) on hydrodynamics and circulation on a sandy beach and, in turn, give insight into their impact on sediment transport processes. Because of the abundance of the available *in situ* measurements, Varkiza coast, in the Saronic Gulf (western Aegean Sea), has been selected as a suitable area for modelling the hydrodynamic and meteorological conditions and estimating sediment transport rates during and after intense sea states/storms by using a 2DH (depth averaged) sediment transport model based on finite volume method. The same model has been applied in relevant recent studies; for instance, in Sulis and Annis (2014), the shoreline stability in the lee of a natural reef was analyzed at a western coast of Sardinia by combining various data sources along with 2D numerical model. Furthermore, in Aouiche et al. (2016), the morphological changes of a Moroccan human-impacted beach were studied during eight successive storm events through hydrodynamic simulations of storm waves and topographic surveys, highlighting the protective role of dunes, the severity of the first storms and the usefulness of wave modelling in longshore sand transport. In similar studies, the propagation of waves and the simulation of currents have been performed with the same modules implemented here; see e.g. Archetti and Zanuttigh (2010), Samaras et al. (2016).

The structure of this work is the following: in Section 2, the study area in the Saronic Gulf is described including a general description of the wider area as regards geographical, morphological and climatological features. The model description is presented in Section 3, along with the most fundamental equations for the three modules included in the model simulations, i.e. the hydrodynamic, spectral wave and sediment transport modules, and the corresponding configuration (i.e. model domain, bathymetry, wind/wave input, etc.). In Section 4, the validation of the adopted model is presented and the obtained results from the 2DH simulations are exhibited and analyzed in Section 5 and a comparison of measured and modelled bed level differences is conducted.

Finally, in Section 6, some suggestions are provided for coastal managers based on the findings of this study while concluding remarks are drawn in the last section.

## 2. Geographical and oceanographic data

Varkiza coast, located in the homonym bay, forms a part of the north-eastern Saronic Gulf, a semi-enclosed embayment in the south-western Aegean Sea; see Fig. 1. It is limited in width and length (around 900 m), while at the east side of the coast there is a flume mouth that follows dry/wet epochs. Furthermore, the U-shape and south orientation of the examined coast confine wave action, which is the primary factor for the settlement of sediments. Erosion phenomena are evident due to both the intensive onshore development and physical conditions.

The main reasons for choosing the particular coast refer to the availability of the following features:

1. *in situ* measurements as regards the wave parameters from two different data sources; an oceanographic buoy at an offshore location and an acoustic wave and current (AWAC) profiler at the entrance of the bay (see also Fig. 1 and Section 4);
2. a detailed bathymetry up to 25 m water depth inside Varkiza Bay, which was partially based on seabed mapping;
3. cross-shore sections along the beach, on which bed level was measured after intense sea states completing an annual cycle, as well as grain size of sediments (Foteinis, 2014; Skanavis, 2013), and;
4. the touristic character of the area, along with the intense socio-economic activities along the beach mainly during summer months, that renders the understanding and prediction of sediment transport phenomenon a critical task.

### 2.1. Bathymetry and coastline

Regarding the bathymetry of the Saronic Gulf, the eastern part has an extended zone with depths up to 100 m and a much gentler bottom slope than the western one, which has depths up to 450 m. Going to the south of the gulf, the bottom depth deepens (approximately up to 240 m) and further south, waters get more shallow again; see also Fig. 3 (left panel). Regarding the sea bed bathymetry of Varkiza Bay, it is rather smooth and shallows gradually towards the coast, decreasing, in turn, the wave energy flux. Moreover, at about 2 m depth, there is a continuous rocky formation at the eastern side of the beach that act as a submerged breakwater.

The feeding mechanism of the beach with debris is relatively limited while sediment transport depends mainly on the wind regime. Varkiza beach is composed of sandy sediments with varying granulometric gradations while in the eastern part of the beach, there are quaternary deposits forming a horizontal layer. The long-term evolution of the coastline from aerial photographs indicates the erosion of the beach up to 20 m at the east side of the beach in the last 70 years (Skanavis, 2013).

### 2.2. Wind and wave climatology

As regards wind and wave climatology, the analysis was based on a 9-year dataset from an oceanographic buoy that was taken into consideration as a representative location for the examined area. This buoy, deployed at the southern part of the Saronikos Gulf (37.58°N–23.55°E, water depth ~200 m) belongs to the POSEIDON marine monitoring network that operates under the responsibility of the Hellenic Centre for Marine Research (HCMR) since 2000 (Soukissian et al., 1999). The wind measurements, with reference height 3 m above

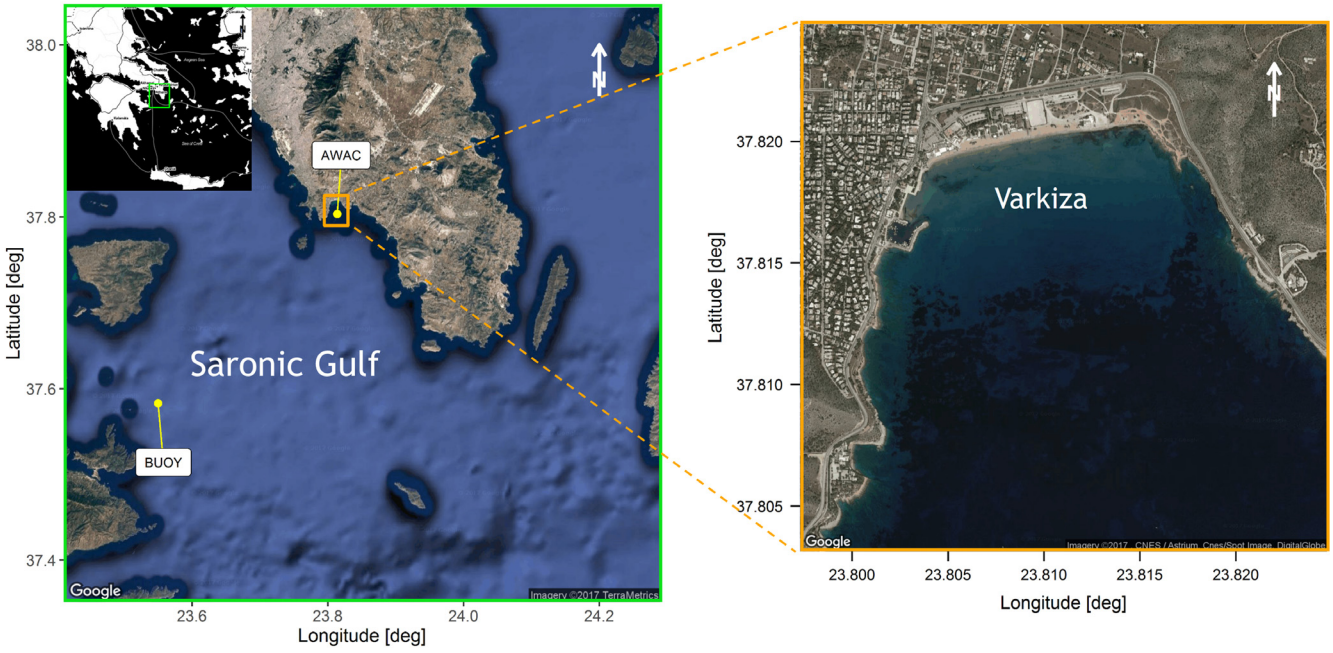


**Figure 1** Aerial map of the Saronic Gulf along with the locations of the *in situ* devices (left panel), and the study area of the coast of Varkiza (right panel) from Google Earth.

sea surface, have a 3-h recording interval with 1 Hz sampling frequency (averaged over a 600-s recording period), while the wave measurements have a 3-h recording interval with 1024 s for the sampling period of the free surface. The time series of wind speed and significant wave height is between 08/2007 and 05/2015.

In Fig. 2, the rose charts of wind speed and significant wave height are presented in the left and right panel, respectively, along with the corresponding frequencies of occurrence. From the former figure, it is illustrated that winds are blowing mainly from the north (sector [337.5, 22.5]) while, at the same sector, high values of wind speed are also present with the maximum one reaching values up to 17.3 m $s^{-1}$. On the other hand, for the latter figure, the prevailing wave directions (sectors [0, 67.5] and [135, 157.5]) correspond to the less frequent wind directions. Large fetches are evident from the eastern side of the location of the buoy (around 65 km) while in the north and south directions, wave fetch is smaller (15 km on the average). Waves propagating from the west have very low frequency of occurrence, which is reflected also by the very small fetch. Low values of significant wave height (up to 0.5 m) have very high frequency of occurrence (4—5%) coming from the east, while waves characterized with the highest values of the same parameter (up to 3.1 m) propagate from the south-east, attributed to the very large fetch (115 km). Furthermore, let us note that the scattering of wind directions is broader compared to the wave directions.

As regards water circulation, in Kontoyiannis (2010) direct current observations were analyzed at three different time periods and it was concluded that the seasonal flows at the north-eastern part of the Gulf have a northward meandering when north-western, western and southern winds are blowing. Furthermore, the circulation pattern is characterized by a two-layer structure (cyclonic in the upper layer and anticyclonic in the lower layer) from late spring to summer to late fall. In the same work, the time series of current velocity for a 3-month period (11/2003—01/2004) indicated that the currents are in the mean rather weak.

## 3. Model description and configuration

In this study, a 2DH model is adopted; such models are deterministic in the sense that they are generally process-based (i.e. they are based on mathematical formulation and assumptions, and the representation of the examined processes is computer-based) and are the most widely used in engineering applications. The basic principles that are applied are the conservation of fluid momentum, wave energy and mass (fluid and sediment). Sediment modelling is established on a depth-averaged hydrodynamic model, a phase-averaged wave model and sediment transport equations. The movement of sediment is based on the Eulerian approach, where suspended sand particles are represented by a concentration and sediment as a continuum (Amoudry and Souza, 2011).

The numerical modelling package that was used for the purpose of this analysis is MIKE 21/3 Coupled Model Flexible Mesh (hereafter MIKE21 CFM) developed by DHI Group (DHI, 2016a, 2016b). This package can be applied to various hydraulic phenomena in lakes, rivers, estuaries, bays, coastal areas and seas through a dynamic modelling system; in the context of this study, it combines three different modules: (i) the hydrodynamic (HD) module; (ii) the spectral wave (SW) module; and (iii) the sand transport (ST) module. The core computational components of MIKE21 CFM are the first two

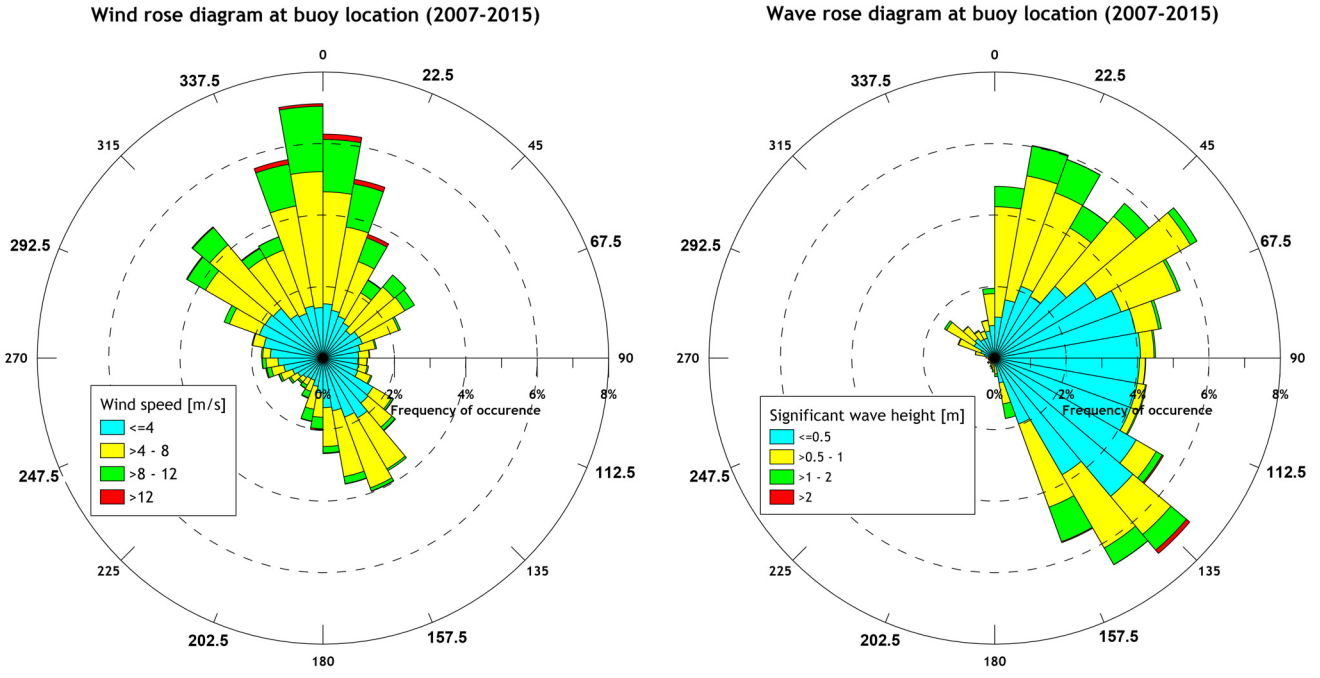


**Figure 2** Rose diagram of wind speed and wind direction (left panel), and significant wave height and wave direction (right panel) at the buoy location for the period 2007—2015.

modules, which simulate the mutual interaction between currents and waves, respectively, using a dynamic coupling. The additional dynamic coupling of the third module can give a full feedback of the bed level changes on waves and flow calculations. Let us note that such models require careful analysis before the final implementation in order to gain the optimum trade-off between computer run times and density of the computational mesh.

### 3.1. Flow (hydrodynamic) and spectral wave modules

The simulation of flows and transports in marine, coastal and estuarine areas is based on a flexible mesh approach, where the corresponding variations are described by the numerical solution of the 2D incompressible Reynolds averaged Navier–Stokes equations under the Boussinesq hypothesis. The continuity equation (in horizontal Cartesian coordinates) over water depth $h = \eta + d$, where $\eta$ is the surface elevation and $d$ the still water depth, is the following:

$$\frac{\partial h}{\partial t} + \frac{\partial h\overline{u}}{\partial x} + \frac{\partial h\overline{v}}{\partial y} = hS^{\mathrm{HD}}, \tag{1}$$

where $t$ is time, $h\overline{u}, h\overline{v}$ denote the depth average values of the velocity components in the $x$, $y$ directions, respectively, and $S^{\mathrm{HD}}$ is the magnitude of discharge due to point sources. The momentum equations for the $x$- and $y$-component, respectively, are the following:

$$\begin{aligned}\frac{\partial h\overline{u}}{\partial t} + \frac{\partial h\overline{u}^2}{\partial x} + \frac{\partial h\overline{v}\overline{u}}{\partial y} &= f\overline{v}h - gh\frac{\partial \eta}{\partial x} - \frac{h}{\rho_0}\frac{\partial p_a}{\partial x} - \frac{gh^2}{2\rho_0}\frac{\partial \rho}{\partial x} \\ &+ \frac{\tau_{sx}}{\rho_0} - \frac{\tau_{bx}}{\rho_0} - \frac{1}{\rho_0}\left(\frac{\partial s_{xx}}{\partial x} + \frac{\partial s_{xy}}{\partial y}\right) \\ &+ \frac{\partial hT_{xx}}{\partial x} + \frac{\partial hT_{xy}}{\partial y} + hu_s S^{\mathrm{HD}},\end{aligned} \tag{2}$$

and

$$\begin{aligned}\frac{\partial h\overline{v}}{\partial t} + \frac{\partial h\overline{u}\overline{v}}{\partial x} + \frac{\partial h\overline{v}^2}{\partial y} &= -f\overline{u}h - gh\frac{\partial \eta}{\partial y} - \frac{h}{\rho_0}\frac{\partial p_a}{\partial y} - \frac{gh^2}{2\rho_0}\frac{\partial \rho}{\partial y} \\ &+ \frac{\tau_{sy}}{\rho_0} - \frac{\tau_{by}}{\rho_0} - \frac{1}{\rho_0}\left(\frac{\partial s_{yx}}{\partial x} + \frac{\partial s_{yy}}{\partial y}\right) \\ &+ \frac{\partial hT_{xy}}{\partial x} + \frac{\partial hT_{yy}}{\partial y} + hv_s S^{\mathrm{HD}},\end{aligned} \tag{3}$$

where $f$ is the Coriolis parameter, $g$ is the gravitational acceleration, $p_a$ is the atmospheric pressure, $\rho_0$ is the reference density of water, $\rho$ is the water density, $s_{xx}$, $s_{xy}$, $s_{yx}$, $s_{yy}$ are the radiation stress components, $T_{xx}$, $T_{xy}$, $T_{yx}$, $T_{yy}$ are the lateral stresses, and $u_s$, $v_s$ are the velocity components at which the water is discharged.

The SW module is a third-generation spectral wind-wave generation model that simulates the growth, decay and transformation of wind-generated waves and swells both in offshore and coastal regions, and is based on unstructured meshes (in the geographical domain). The above simulations are based on the conservation equation of the wave action that is written as (Komen et al., 1994):

$$\frac{\partial N}{\partial t} + \nabla\cdot(\overline{v}N) = \frac{S_{\mathrm{tot}}^{\mathrm{SW}}}{\sigma}, \tag{4}$$

where $N(\overline{x}, \sigma, \theta, t)$ is the wave action density in the horizontal Cartesian coordinates $\overline{x} = (x, y)$, equal to $N = E/\sigma$, with $E$ being the directional distribution of energy density, $\sigma$ is the relative angular (intrinsic) frequency and $\theta$ the direction of each component in the spectrum. Moreover, $\overline{v} = (c_x, c_y, c_\sigma, c_\theta)$ is the wave propagation velocity in the 4D phase space $(\overline{x}, \sigma, \theta)$, $\bigtriangledown$ is the 4D differential operator, and $S_{\mathrm{tot}}^{\mathrm{SW}}$ is the source term of wave energy balance representing a large number of physical processes. The physical phenomena that are included are the following:

- wave growth by wind action $S_{\mathrm{in}}^{\mathrm{SW}}$, proposed by the theory developed by Janssen in a series of studies (Janssen, 1989, 1991; Janssen et al., 1989) as regards wind and wave interaction;
- wave energy transfer due to non-linear wave-wave interaction $S_{\mathrm{nl}}^{\mathrm{SW}}$, using the Discrete Interaction Approximation (DIA) of Hasselmann et al. (1985);
- dissipation of wave energy due to white-capping $S_{\mathrm{wc}}^{\mathrm{SW}}$, proposed by Hasselmann (1974) and tuned according to Janssen (1992);
- dissipation of wave energy due to bottom friction $S_{\mathrm{bf}}^{\mathrm{SW}}$, based on the approach of Johnson and Kofoed-Hansen (2000), which takes into consideration wave and sediment properties;
- dissipation of wave energy due to wave breaking $S_{\mathrm{wb}}^{\mathrm{SW}}$, based on the breaking model of Battjes and Janssen (1978), and Eldeberky and Battjes (1996).

For the discretization of the governing equation in the geographical and spectral space, a cell-centred finite volume method is used by subdividing the continuum into non-overlapping elements, while a fractional step method is applied for the time integration. As regards the time formulation of the SW module, the instationary mode was selected.

### 3.2. Sediment transport module

The modelling of non-cohesive sediment transport field can be obtained by using the theory of combined wave and current. This module can be applied in coastal regions, such as estuaries, tidal inlets and coasts, as well as in coastal structures, such as harbours. Let us note that apart from the hydrodynamic/wave conditions of an area, the pattern of sediment transport is also influenced by the characteristics of the transported material, usually defined by grain diameter, gradation, grain (relative and bulk) density, porosity, fall velocity, etc.

The total sediment transport $q_{\mathrm{tot}}$ is usually defined by the bed load transport $q_{\mathrm{b}}$ (i.e. load that is in continuous contact with the seabed during transport) and the sediment transport in suspension $q_s$ (i.e. load that is moving without being in contact with the seabed due to the turbulent flow). Wash load (i.e. finer suspended material than that of the seabed that remain in permanent suspension) is considered negligible in the coastal environment and is not included in this module.

As regards the bed load transport, it is calculated from the instantaneous Shields parameter based on the model that was proposed by Engelund and Fredsøe (1976). Among the parameters that affect bed load transport are the hydraulic features, such as shear stress, average velocity, and the geometric ones, such as bed slope, grain-size distribution

(Poorhosein et al., 2014). The suspended sediment transport is the result of the product of the time-averaged instantaneous flow velocities $u$ and the instantaneous sediment concentration $c$ by integrating over the local water depth $D$:

$$q_s = \frac{1}{T}\int_0^T \int_{2d}^{D} (uc)\, dz\, dt, \tag{5}$$

where $d$ is the characteristic grain diameter, usually equal to the median grain diameter $d_{50}$.

The determination of the bed level change at each element is based on the Exner equation (sediment continuity equation) that is written (in horizontal Cartesian coordinates) as follows:

$$-(1-n)\frac{\partial z_b}{\partial t} = \frac{\partial S_x^{ST}}{\partial x} + \frac{\partial S_y^{ST}}{\partial y} - \Delta S^{ST}, \tag{6}$$

where $n$ is the bed porosity, $z_b$ is the bed level, $t$ is time, $S_x^{ST}$ and $S_y^{ST}$ are the total load transport in the $x$ and $y$ direction, respectively, and $S^{ST}$ is the sediment source/sink rate. For an equilibrium description, the source/sink term is set to zero, unless lateral sediment supply is considered.

The sediment transport rates are found by linear interpolation from a sediment transport table, which is calculated in advance in order to speed up the calculations. Based on equilibrium sediment transport method, the values of this table are derived from a quasi-3D numerical model (STPQ3D), which calculates in the two horizontal dimensions (longshore and cross-shore) time-averaged and instantaneous hydrodynamic flow conditions that drive sediment transport algorithms; see Elfrink et al. (1996). The integrated momentum approach of Fredsøe (1984) is used for the time integration of the boundary layer.

## 3.3. Model configuration

### 3.3.1. Model domain and bathymetric data

In order to manage the computational domain and economize on computation time, the model domain was sectioned into six nested rectangles, going gradually from the outer area (i.e. level 1) up to the entrance of Varkiza Bay (i.e. level 6); see also Fig. 3 (right panel) for the representation of the different levels. The outer area covers a surface of 45 km × 76 km and the area of Varkiza Bay equals to 2 km × 2.5 km.

In order to determine the variability of flow characteristics in space, model grid resolution is a key factor that affects the quality of the obtained results. The provision of flexible mesh in MIKE21 results to a more accurate representation of the area under study, with the choice of finer

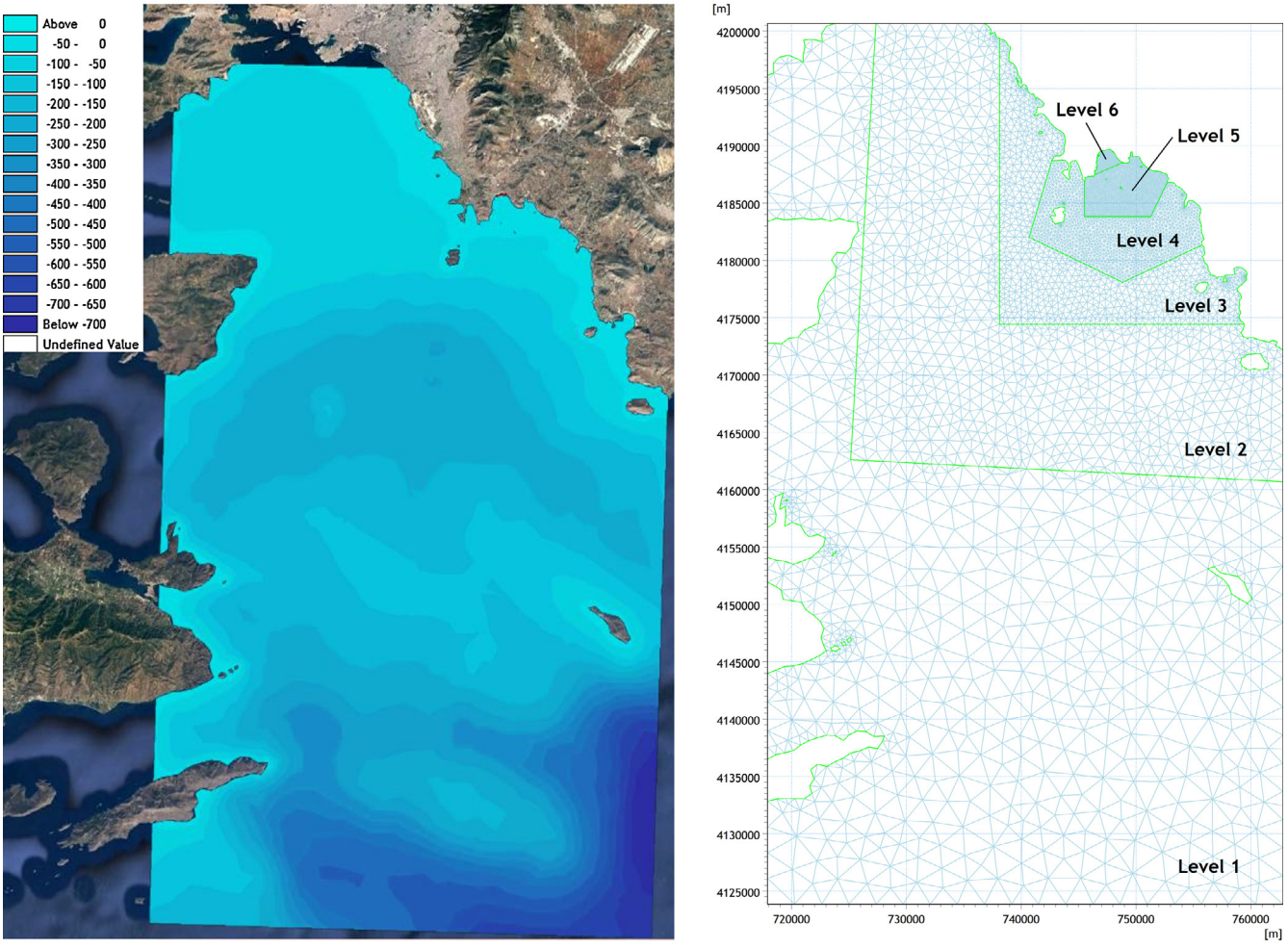


**Figure 3** The model domain showing the bathymetry of the examined area (left panel) and the mesh grid for the adopted levels (right panel).

mesh elements at local areas of special interest. In this study, various mesh areas were applied to discretise the water surface, with small triangular elements representing areas where the accuracy in the calculations was important. The final mesh area of the examined area is presented in the right panel of Fig. 3.

The bathymetric information that is necessary for constructing the mesh area for the entire area was obtained by the Hellenic Navy Hydrographic Service (HNHS) from maps of different spatial scales. The bathymetric grid data for the last level (of a 5-m spatial resolution) was obtained by combining a high-resolution map from the HNHS and field measurements provided by the HCMR. In Fig. 3 (left panel), the 2D bathymetric representation of the examined area is displayed in Google Earth; the deepest water depth is close to 800 m at the south-eastern boundary of the study area.

### 3.3.2. Input data

In this section, the boundary conditions used as input for the model simulations are described for each module, along with some determinative parameters. Let us note in advance that the simulation results are provided simultaneously for all levels of the model domain; forcing imposed at the boundaries of the model generates flow and wave conditions inside the outmost level, which in turn define the corresponding boundary conditions of the next level up to the inmost one.

The period of the simulation, extending from January 3 to February 19, 2013, was selected so as to include a sequence of extreme events with significant wave heights higher than 2.5 m that were recorded at the entrance of the bay during this period (see also Fig. 6). Furthermore, bathymetry resolution (including flexible mesh) and time step for computations of the HD and SW results are key parameters for the purpose of this study. As concerns the mesh we note that it becomes progressively finer as we move from level 1 to level 6, which is the local domain at the coastal site of Varkiza. The total number of elements in the whole domain is 12,176, the corresponding number of elements in level 6 is 1600, and the time step is set to $\Delta t$ = 1800 s. The latter are found to be enough for numerical convergence of the results concerning the wave quantities that are presented in more detail below. Specifically, numerical investigation shows that the calculated results do not change more than 5% with further enhancement of the mesh at the different subdomains and reduction of the time step.

The necessary input data for the HD module include the following parameters: wind forcing, radiation stress fields, boundary conditions, atmospheric pressure, bed resistance and eddy viscosity. Eddy viscosity was obtained in the domain from the Smagorinsky formulation with a constant coefficient (equal to 0.28), bed resistance (defined by the Manning number) was only varying at level 6 (with values between 32 $m^{1/3}\,s^{-1}$), where sediment transport rate is of interest, while salinity and temperature were constant during the simulation (barotropic mode). Regarding boundary conditions, normal fluxes were forced to zero for all variables along both closed and open boundaries, assuming full slip boundary conditions, since all boundaries are far from the area of interest and tidal heights are rather small and do not impact the simulation results. Let us note that tidal heights, predicted from the Global Tide Model Data, were also used as an alternative input for the open boundaries; however, the simulation results were similar to the ones presented in this work.

The effect of the wind forcing on the flow field is included by considering wind speed and wind direction; in this way, wind shear stress is calculated on the water surface. For the numerical simulations, these two variables were considered to be varying in time but constant in domain. Wind speed and direction were obtained by the results of the POSEIDON II weather forecasting system (Papadopoulos et al., 2008) that has been developed in the framework of the POSEIDON-II project[1] (2005–2008).

As regards the SW module, the corresponding conditions at the offshore (south) open boundary were varying in space (along the wave generation line) and time. The corresponding input was based on the WAM Cycle-4 code, a third generation wave model, which computes spectra of random short-crested wind-generated waves. The spatial resolution is $1/30^\circ \times 1/30^\circ$ ($\sim$3 km) resolving the wave spectrum at each grid point in 24 directional and 30 frequency bins. The wave parameters that were obtained are the significant wave height $H_{m0}$, the peak wave period $T_p$, the mean wave direction $\theta_{\text{wave}}$ and directional spreading $n$. The zero up-crossing period $T_z$, obtained from the WAM model, was converted to the peak wave period $T_p$ by using the following approximate relation:

$$\frac{T_z}{T_p} = 0.6673 + 0.05037\gamma - 0.006230\gamma^2 + 0.0003341\gamma^3, \qquad (7)$$

where $\gamma$ is the peak enhancement factor of the spectrum. Assuming a JONSWAP spectrum with $\gamma = 3.3$, Eq. (7) results in $T_p = 1.2859T_z$.

Other key parameters or coefficients for setting SW module are:

- energy transfer, where quadruplet-wave interaction was considered;
- wave breaking was included by specifying the gamma parameter $\gamma_{\text{wb}}$ (constant in domain, equal to 0.8);
- bottom friction, specified by the Nikurdase roughness $k_N$ (constant in domain, equal to 0.04 m);
- white capping, specified by the two dissipation coefficients (constant in domain) $C_{\text{dis}}$, which controls the overall dissipation rate (set to 4.0), and $DELTA_{\text{dis}}$, which controls the weight of the dissipation in the energy spectrum (set to 1.0).

Let us note that both wind and wave data were derived from the POSEIDON Live Access Server (LAS, http://poseidon.hcmr.gr/listview.php?id=17), which is a gateway to archived model results, dating from December 1, 2012 to June 30, 2013 with a 6-h time resolution for both datasets. Missing data were filled in by linear interpolation to allow the execution of the simulation; however, interpretation of the simulation results during these time periods should be avoided.

Finally, regarding the setting up of the ST module, the transport tables have a key role; these tables are built based

[1] The POSEIDON-II weather forecasting system is operational since December 2007 and is applied on a horizontal resolution of $1/20^\circ \times 1/20^\circ$ ($\sim$5 km) over the domain covering the whole Mediterranean and Black Sea regions and the surrounding countries.

on all possible combinations according to the specified intervals of the involved parameters (i.e. the root-mean square wave height, peak period, current speed, wave height-to-water depth ratio, angle between current and waves, median grain diameter $d_{50}$ and sediment grading). Additional parameters that are important for this module are forcing from the wave and current action, provided by the HD and SW simulations (see below Fig. 7 and Fig. 8, respectively), sediment properties, time step factor (set to 5, i.e. estimation of bed level and sediment transport every 5th HD time step) and settings for the morphological changes and boundary conditions of the area of interest. In particular, based on measured data, the spatial distribution of the grain diameter of the sediment ($d_{50}$) over the coastal zone of Varkiza Bay was set to 2 mm for water depths greater than 20 m (where no significant sediment transport is expected). Moreover, in depths less than 3 m there is a gradual increase of $d_{50}$ from 0.1 mm to 0.4 mm in the S-N direction (moving towards the shoreline), and a variation from 0.35 mm to 0.45 mm in the E-W direction on the shore. Sediment grading was kept constant (equal to 1.45) for the same level.

## 4. Model calibration and validation

The simplifying assumptions that are included in order to attenuate the time-consuming and computer power demanding numerical solutions when describing coastal processes, like sediment transport, generate some limitations as regards applicability; thus, they lead to the partial description of real-world cases, and introduces uncertainties. Calibration and validation of the model from *in situ* measurements is an inextricable procedure in the context of numerical modelling in order to obtain reasonable estimations (Simons et al., 2000) and improve reliability and ability of the proposed model to predict such cases.

Model calibration is necessary in order to adjust and improve the agreement between the results of the model simulations and a chosen set of benchmarks (Trucano et al., 2006); in our case, benchmark is a data set obtained by *in situ* measuring devices, which are considered to be the most accurate data sources. On the other hand, validation is the process of verifying that the predictions from the model are consistent with the examined physical events after calibrating the involved parameters or coefficients. Let us note that the data used for the validation should be different from the data used during the calibration phase.

In this work, calibration was based only on the wave parameters, since no current data were available during this period of time. The available *in situ* measurements were taken from an oceanographic buoy and an AWAC sensor for the period between January 1 and March 22, 2013. The locations of the two measuring devices are depicted in Fig. 1. As mentioned in Section 3.3.2, there are a number of parameters and coefficients that should be set so that the model predicts reasonable results. The parameters that influenced the model results in the case of the fully spectral formulation and should be adjusted were $C_{DIS}$ and $DELTA_{DIS}$ dissipation coefficients, gamma and alpha parameters of wave breaking and bottom roughness.

The wave parameters that were used to calibrate the model were the significant wave height, the (zero-crossing or peak) wave period and the mean wave direction at the buoy and AWAC locations. The above-mentioned parameters were investigated for a variety of combinations in order to achieve the optimum result. Let us remark that in the calibration procedure, more emphasis was given to the significant wave height, since highest waves are expected to have major contribution to the movement of sediments during storm events. The optimum agreement between *in situ* measurements and model results was obtained after applying some additional statistical measures for the assessment of the model.

Specifically, the following statistical measures were applied for the linear variables (i.e. significant wave height and wave period):

the root mean square error (RMSE),

$$\mathrm{RMSE} = \sqrt{\frac{1}{n}\sum_{i=1}^{n}(x_{\mathrm{sim}} - x_{\mathrm{obs}})^2}, \tag{8}$$

and, the mean absolute error (MAE),

$$\mathrm{MAE} = \frac{1}{n}\sum_{i=1}^{n}|x_{\mathrm{sim}} - x_{\mathrm{obs}}|, \tag{9}$$

where $x_{\mathrm{sim}}$ is the value of the examined linear variable obtained from the model simulation, $x_{\mathrm{obs}}$ is the corresponding value from the *in situ* measurements and $n$ is the sample size. RMSE and MAE have the same units as the variable being estimated.

The corresponding statistical measures for the examined directional variables (i.e. mean wave direction) are defined as follows:

the mean circular absolute error (MCAE) (Jing-Jing et al., 2014),

$$\mathrm{MCAE} = \frac{1}{n}\sum_{i=1}^{n}|d_1(\theta_{\mathrm{sim}}, \theta_{\mathrm{obs}})|, \tag{10}$$

and the root mean error (RME) (Karathanasi et al., 2016),

$$\mathrm{RME} = \sqrt{-2\ln\left(\frac{1}{n}\sum_{i=1}^{n}\left|\cos\left(\frac{\theta_{\mathrm{sim}} - \theta_{\mathrm{obs}}}{2}\right)\right|\right)}, \tag{11}$$

where $\theta_{\mathrm{sim}}$ is the value of the examined directional variable obtained from the model simulation, $\theta_{\mathrm{obs}}$ is the corresponding value from the *in situ* measurements and $d_1$ denotes the (minimum) difference between two angles and is equal to $\pi - |\pi - |\theta_{\mathrm{sim}} - \theta_{\mathrm{obs}}||$. The values of MCAE are in radians while RME is dimensionless.

A good agreement between the measurement and the results from the simulation is achieved if the values of the above mentioned criteria are as close as possible to zero.

### 4.1. Results compared with buoy measurements

Regarding the buoy records, the wave parameters that were used to calibrate the model were the significant wave height, the zero-crossing wave period and the mean wave direction. The time period for the model simulation as regards the calibration procedure from these measurements was between February 20 and March 20, 2013.

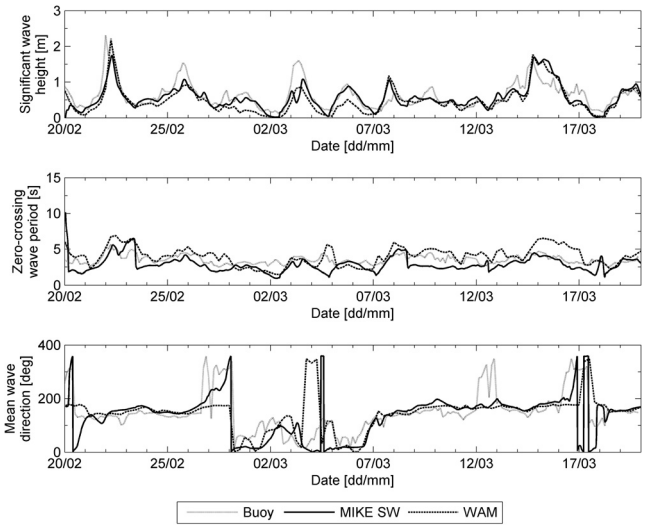


**Figure 4** Time series of buoy measurements and results from WAM and MIKE SW at the buoy location for significant wave height (upper panel), zero-crossing wave period (middle panel) and mean wave direction (lower panel).

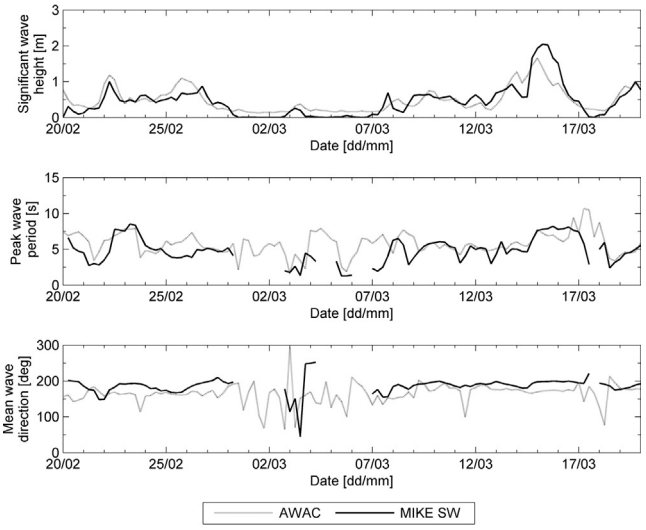


**Figure 5** Time series of AWAC measurements and model data for significant wave height (upper panel), peak wave period (middle panel) and mean wave direction (lower panel).

In Fig. 4, the time series of simulated (black solid line corresponds to the MIKE SW results and black dashed line corresponds to the WAM results) and measured (grey line corresponds to buoy records) wave parameters are presented. The agreement of the results between MIKE SW and WAM is generally better for significant wave height and mean wave direction compared to the buoy measurements and MIKE SW results. The adopted statistical measures, presented in Table 1, illustrate the same situation; (i) for significant wave height, the lowest values of RMSE (0.786 m) and MAE (0.134 m) correspond to the former pair; (ii) for zero-crossing wave period, the lowest values of RMSE (9.710 s) and MAE (0.861 s) are estimated for the former pair; and (iii) for mean wave direction, the lowest values of RME (0.373) and MCAE (0.436 rad) correspond to the former pair. Let us note that the highest discrepancies for zero-crossing wave period between buoy measurements and MIKE SW results are detected for wave heights lower than 0.5 m.

### 4.2. Results compared with AWAC measurements

Regarding the AWAC records, they were used as supplement to the calibration procedure in the sense that the adjusted parameters of the model were kept the same as before. In this case, the examined wave parameters were the significant wave height, the peak wave period and the mean wave direction while the time period for the comparison of the two different datasets was the same as in Section 4.1.

The obtained results between the simulated and the measured parameters are shown in Fig. 5, while the values of the adopted statistical measures are presented in Table 2. The compared time series suggest a good agreement as regards significant wave height and mean wave direction, but peak wave period exhibits a less accurate performance.

**Table 1** Statistical measures as regards wave parameters between buoy data and MIKE SW results, and WAM and MIKE SW results at the buoy location.

| **Significant wave height** | **RMSE [m]** | **MAE [m]** |
|---|---|---|
| Buoy-MIKE SW | 1.128 | 0.182 |
| WAM-MIKE SW | 0.786 | 0.134 |
| **Zero-crossing wave period** | **RMSE [s]** | **MAE [s]** |
| Buoy-MIKE SW | 9.710 | 0.861 |
| WAM-MIKE SW | 12.393 | 1.265 |
| **Mean wave direction** | **RME [–]** | **MCAE [rad]** |
| Buoy-MIKE SW | 0.439 | 0.639 |
| WAM-MIKE SW | 0.373 | 0.436 |

## 5. Results

The following results represent the current and wave characteristics and bottom morphology of the examined area for the “extreme” event that occurred on January 18, 2013. In Fig. 6, the time series of wind speed, wind direction and significant wave height used as input at the offshore boundary are presented. It is evident that southern winds generate the highest values of significant wave height during the simulation period. Moreover, wave height variation is found to be in good agreement with wind speed data, denoting that the waves at this location are mostly wind generated.

**Table 2** Statistical measures as regards wave parameters between AWAC data and MIKE SW results at the AWAC location.

| **Significant wave height** | **RMSE [m]** | **MAE [m]** |
|---|---|---|
| AWAC-MIKE SW | 0.504 | 0.192 |
| **Zero-crossing wave period** | **RMSE [s]** | **MAE [s]** |
| AWAC-MIKE SW | 8.905 | 1.403 |
| **Mean wave direction** | **RME [–]** | **MCAE [rad]** |
| AWAC-MIKE SW | 0.364 | 0.508 |

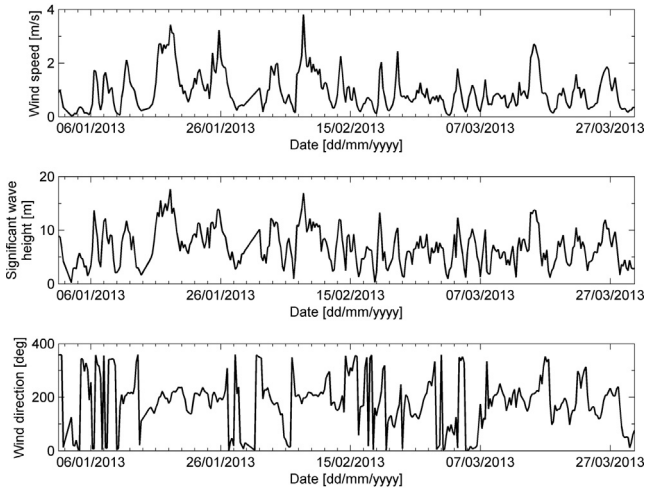


**Figure 6** Time series of wind speed (upper panel), significant wave height (middle panel) and wind direction (lower panel) that were used as input at the south boundary during the model simulation.

## 5.1. HD results

The spatial distribution of current speed and the corresponding direction for the entire area and the coast of interest is depicted in Fig. 7 during a specific extreme event (on January 18, 2013) that was characterized mainly by south wind and wave directions. The model domain is characterized by low current speeds, of the order of 0.2 m $s^{-1}$. As regards Varkiza Bay, highest values of current speed are observed; locally (at the east side of the bay) current speed reach values up to 0.9 m $s^{-1}$, which is an extreme value encountered very locally during the peak of the storm. The latter high values may be also attributed to the wave direction and the orientation of the coastline. Moreover, in the right panel of Fig. 7 a counter-clockwise current circulation is evident during this extreme event due to the concave and curvilinear shoreline structure of Varkiza coast and the relatively deep water depths that enhance penetration of waves and currents from easterly sectors. The combination of the above factors produces offshore currents near the western part of the study area. From the analysis, it seems that tidal currents might be of secondary importance in the context of coastal erosion.

## 5.2. SW results

In Fig. 8 and Fig. 9, the spatial distribution of the significant wave height and mean wave period, respectively, are presented over the model domain. The analysis of the results shows that the significant wave height is reduced as the waves propagate towards the shallower water depths of Varkiza beach; see also right panel of Fig. 8. Near the coast the wave height is lower than 2 m with a mean wave period around 7 s; see also right panel of Fig. 9.

## 5.3. ST results

In the left panel of Fig. 10, the spatial distribution of the bed level change at the specific time step is presented. Based on

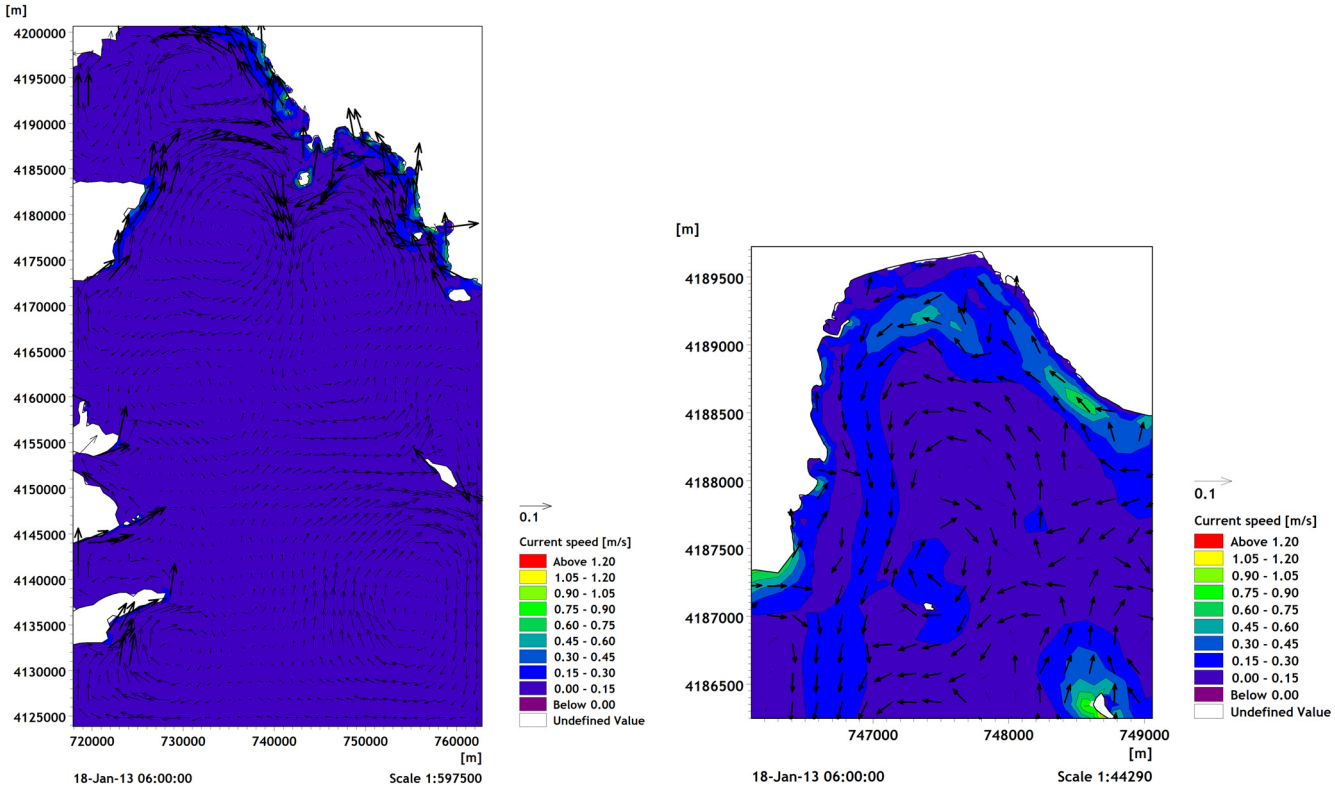


**Figure 7** Spatial distribution of current speed and current direction for the entire model domain (left panel) and for Varkiza Bay (right panel) at a specific time step of the simulation.

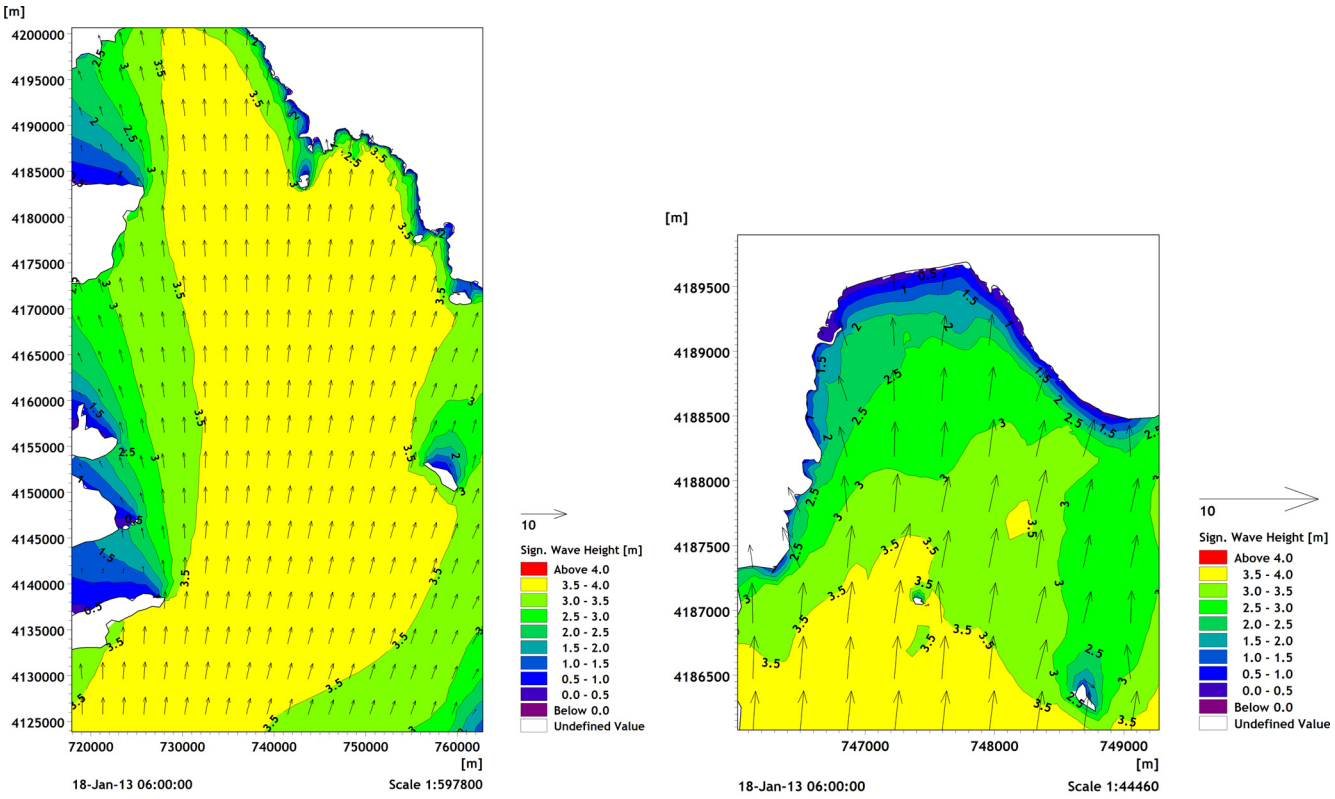


**Figure 8** Spatial distribution of significant wave height for the entire model domain (left panel) and for Varkiza Bay (right panel) at a specific time step of the simulation.

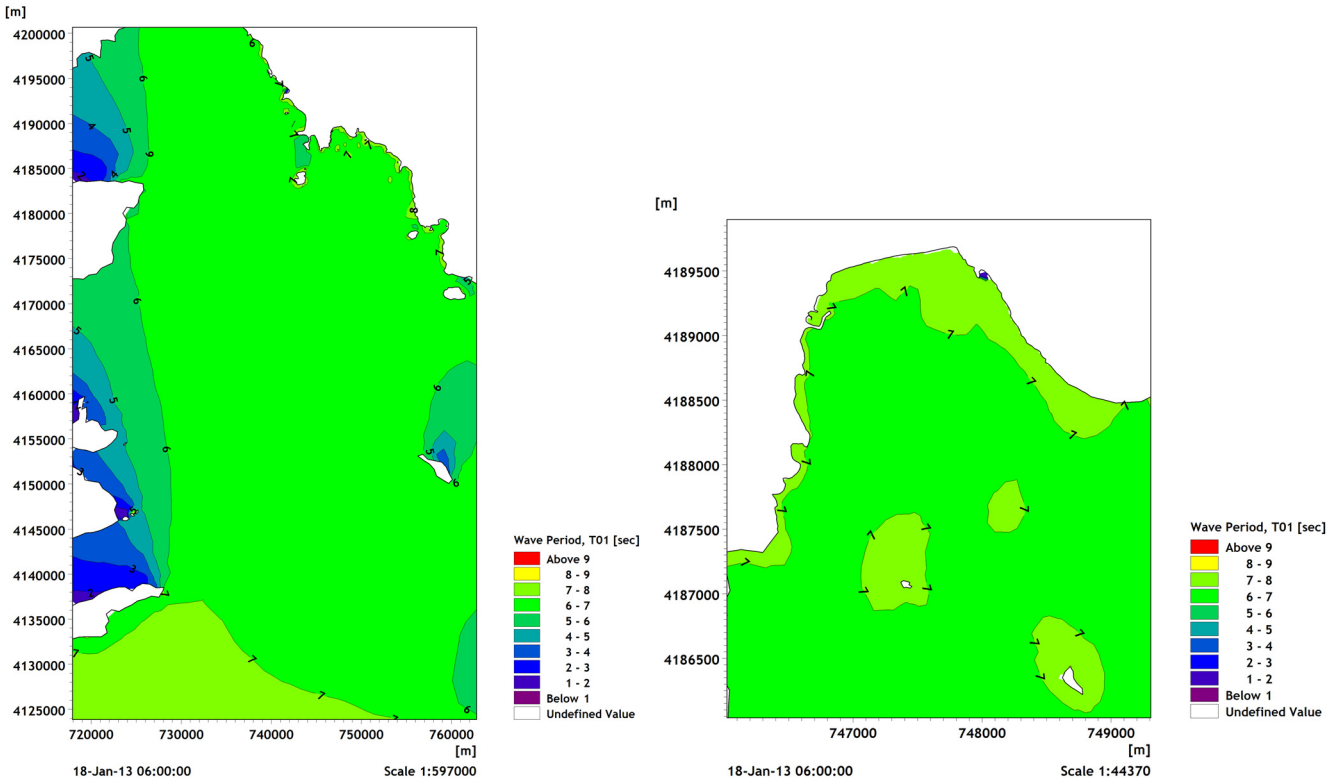


**Figure 9** Spatial distribution of mean wave period for the entire model domain (left panel) and for Varkiza Bay (right panel) at a specific time step of the simulation.

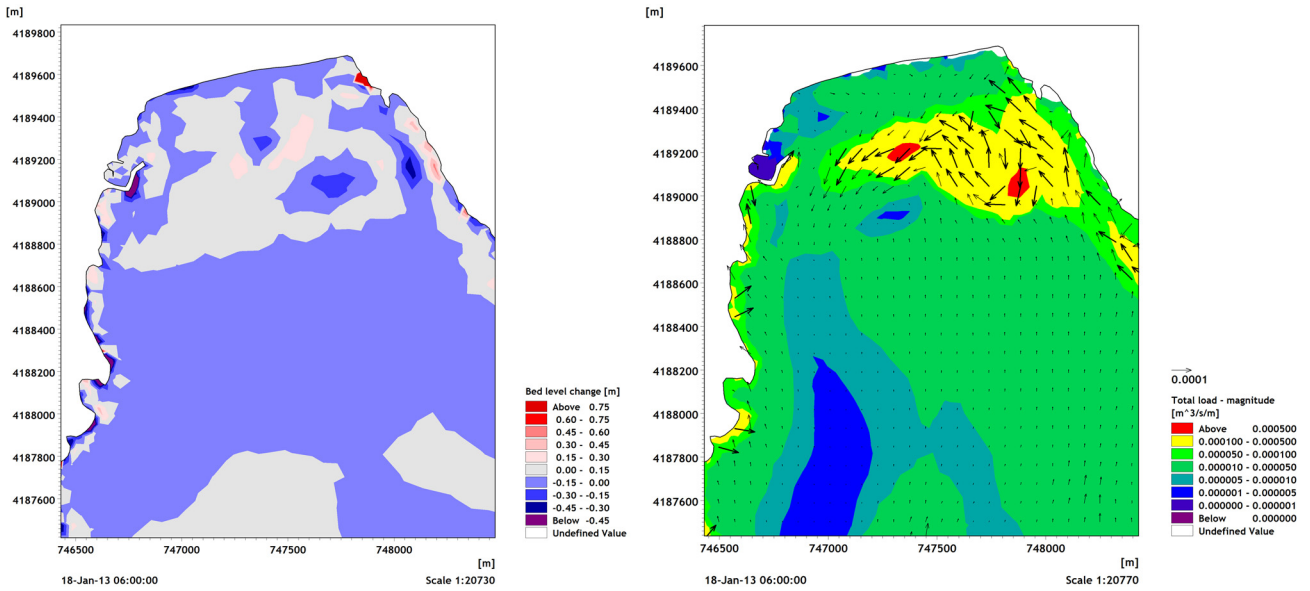


**Figure 10** Spatial distribution of bed level change (left panel) and total magnitude of sediment transport (right panel) for Varkiza Bay at a specific time step of the simulation.

the simulation results, negative bed level changes (up to −0.3 m) are observed along the coastline of the examined beach, while off the coast of Varkiza the corresponding bed level changes are relatively smaller. Positive bed level changes are depicted mainly along the east side of Varkiza Bay that may be attributed to the high values of current speed.

In the right panel of Fig. 10, the total load of sand transport is presented, along with the corresponding direction, for the examined extreme event. The highest values of sand transport (up to 0.00098 $m^3$ $(s\,m)^{-1}$) are depicted mainly at the 4-m isobath at the central and eastern side of the beach, denoting erosion trend at a larger spatial scale compared to the west side. In the western part of the beach, at a zone of 150 m width from the coastline, accretion patterns are encountered while the rest zone is characterized by erosion. The same behaviour was revealed and discussed in the study of Skanavis (2013), where cross-shore profiles were obtained from a topographical survey by using RTK-GPS, and six sections (section A to F going from east to west, respectively) were presented along Varkiza beach before and after extreme events. In this work, three out of six cross-shore profiles, shown in Fig. 11 (upper panel), are examined with reference to the period from January 5 to February 18, 2013.

In Fig. 11, the bed level change at the cross-shore sections (A,C,E) between the two examined dates (close to the beginning and end of the simulation period) is plotted, along with the initial section bathymetry. The changes calculated by the model are shown by using solid lines and the measured data by using symbols. It is revealed that at all the examined sections there is a clear erosional trend alongshore apart from the field measurements at section E, where accretion is observed for a distance approximately 15 m from the shoreline.

## 6. Discussion

Over the last 50 years, the human activities taken place in Varkiza, such as the construction of a high-traffic coastal avenue parallel to the beach at a distance about 180 m, and marine structures for mooring small boats and the needs of the local fishery community at the west side of the coast, have disturbed gradually the natural equilibrium between coastal hydrodynamics and sediment transport processes, and coastal configuration as well.

Based on the main findings of this study and the overview of the hydrodynamic conditions and wave climate of the beach, coastal protection measures and mitigation methods for coastal erosion at the examined area can be roughly suggested. As was stated by Bergillos et al. (2017), sustainable and economical interventions are preferred for coastal erosion problems; such countermeasures include, among others, beach nourishment (or beach fill), artificial reefs and coral transplantation known as soft engineering methods while breakwaters and other engineering structures belong to the hard engineering measures (Luo et al., 2016). The implementation of the former measures is also enhanced by the topography of Varkiza beach, since pocket beaches suffer less from lateral volumetric losses compared to open and extensive sandy beaches. Whichever countermeasures will be adopted by the collaboration of coastal managers, scientists, decision makers and local authorities for the sustainable development and effective management of this coastal zone, previous extended video monitoring of the beach conditions, including periodically updated bathymetric data, is suggested. Furthermore, advanced local-scale shoreline evolution models, as e.g. UNIBEST (https://www.deltares.nl/en/software/unibest-cl/#8), requiring quite more detailed sedimentological information, allow for precise quantification of the sediment transport rates close to the shoreline.

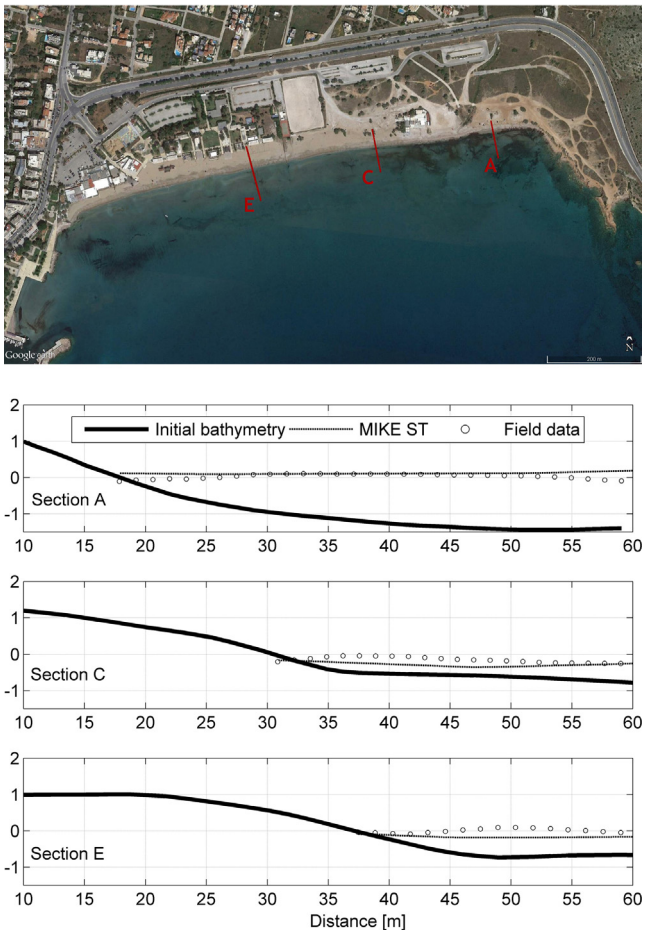


**Figure 11** Locations of cross-shore sections at Varkiza beach (from Google Earth) (upper panel). Initial bathymetry (January 5, 2013) shown by thick solid lines, and bed level differences along the cross-shore sections A, C, E between January 5 and February 18, 2013, as obtained from the model simulation (thin lines) and measured field data (circles).

## 7. Conclusions

In this paper the effects of high waves on sandy beaches and their impact on sediment transport is examined under the simultaneous action of currents and waves. In particular, a 2DH dynamic modelling system is used for simulating the hydrodynamic and wave characteristics of the Saronic Gulf, focusing on Varkiza coast, in order to model hydrodynamic conditions and predict sediment transport phenomena under intense sea wave states. The determination of those characteristics was achieved through the coupling of the flow and spectral wave models by solving the 2D shallow water equations with radiation stress field and the wave-action conservation equation, respectively. The flow, wave and sediment transport equations are solved by using a finite volume method based on non-overlapping triangular elements.

Time series of wind and wave data were taken into consideration as input in the open boundaries of the model domain while the model was calibrated and validated from the available *in situ* measurements through four (linear and directional) statistical measures. The good agreement of the numerical results with *in situ* measurements confirmed the suitability of the model for the assessment and prediction of sediment transport fields at Varkiza beach under the action of high waves. Results from the present analysis showed that offshore currents close to the western side of the examined beach are produced due to the counter-clockwise current circulation and the relatively deep seabed that enhances penetration of waves and currents from easterly sectors. Furthermore, high waves cause erosion along the major part of Varkiza coast while accretion is evident at the western part. Future work will focus on the exploitation of present hydrodynamic computations as input to local-scale shoreline evolution models supporting the detailed lithodynamic investigation of the studied site.

## Acknowledgments

Flora E. Karathanasi would like to thank the GIS section of the HCMR for providing the digitized bathymetric data, and F. Gad for the fruitful conversations on the 2DH model. The authors are also thankful to E. Moussoulis from DHI-Greece for providing the software licence and for his prompt feedback to the raised questions as regards model configuration and optimization, and the two anonymous reviewers for their insightful comments and suggestions.

## References

Amoudry, L.O., Souza, A.J., 2011. Deterministic coastal morphological and sediment transport modeling: a review and discussion. Rev. Geophys. 49 (2), RG2002, http://dx.doi.org/10.1029/2010RG000341.

Aouiche, I., Daoudi, L., Anthony, E.J., Sedrati, M., Harti, A., Ziane, E., 2016. The impact of storms in the morphodynamic evolution of a human-impacted semi-sheltered beach (Agadir Bay, Morocco). J. Afr. Earth Sci. 115, 32–47.

Archetti, R., Zanuttigh, B., 2010. Integrated monitoring of the hydro-morphodynamics of a beach protected by low crested detached breakwaters. Coast. Eng. 57 (10), 879–891, http://dx.doi.org/10.1016/j.coastaleng.2010.05.002.

Bai, Y., Wang, Z., Shen, H., 2003. Three-dimensional modelling of sediment transport and the effects of dredging in the Haihe Estuary. Estuar. Coast. Shelf Sci. 56 (1), 175–186, http://dx.doi.org/10.1016/S0272-7714(02)00155-5.

Battjes, J.A., Janssen, J.P.F.M., 1978. Energy loss and set-up due to breaking random waves. In: Proceedings of the 16th Conference on Coastal Engineering, ASCE, Hamburg, Germany, 569–587.

Bergillos, R.J., Rodríguez-Delgado, C., Ortega-Sánchez, M., 2017. Advances in management tools for modeling artificial nourishments in mixed beaches. J. Marine Syst. 172, 1–13, http://dx.doi.org/10.1016/j.jmarsys.2017.02.009.

Bernabeu, A.M., Medina, R., Vidal, C., 2003. Wave reflection on natural beaches: an equilibrium beach profile model. Estuar. Coast. Shelf Sci. 57 (4), 577–585, http://dx.doi.org/10.1016/S0272-7714(02)00393-1.

Callaghan, D.P., Roshanka, R., Andrew, S., 2009. Quantifying the storm erosion hazard for coastal planning. Coast. Eng. 56 (1), 90–93, http://dx.doi.org/10.1016/j.coastaleng.2008.10.003.

Chen, J.-L., Shi, F., Hsu, T.-J., Kirby, J.T., 2014. NearCoM-TVD – a quasi-3D nearshore circulation and sediment transport model. Coast. Eng. 91, 200–212, http://dx.doi.org/10.1016/j.coastaleng.2014.06.002.

Coco, G., Senechal, N., Rejas, A., Bryan, K.R., Capo, S., Parisot, J.P., Brown, J.A., MacMahan, J.H.M., 2014. Beach response to a sequence of extreme storms. Geomorphology 204, 493–501, http://dx.doi.org/10.1016/j.geomorph.2013.08.028.

Cowell, P.J., Thom, B.G., 1994. Morphodynamics of coastal evolution. In: Carter, R.W.G., Woodroffe, C.D. (Eds.), Coastal Evolution: Late Quaternary Shoreline Morphodynamics. Cambridge Univ. Press, Cambridge, 517 pp.

DHI, 2016a. MIKE 21 & MIKE 3 Flow Model FM, Hydrodynamic and Transport, Scientific documentation.

DHI, 2016b. MIKE 21 Spectral Wave Module, Scientific documentation.

Dibajnia, M., Nairn, R.B., Ross, P., 2004. Analysis of long-term sand accumulation at a harbor using 2DH numerical simulation. Coast. Eng. 51 (8–9), 863–882, http://dx.doi.org/10.1016/j.coastaleng.2004.07.013.

Dodd, N., Blondeaux, P., Calvete, D., de Swart, H.E., Falqués, A., Hulscher, S.J.M.H., Rózyński, G., Vittori, G., 2003. Understanding coastal morphodynamics using stability methods. J. Coastal Res. 19 (4), 849–865.

El Kadi Abderrezzak, K., Die Moran, A., Tassi, P., Ata, R., Hervouet, J.-M., 2016. Modelling river bank erosion using a 2D depth-averaged numerical model of flow and non-cohesive, non-uniform sediment transport. Adv. Water Resour. 93, 75–88, http://dx.doi.org/10.1016/j.advwatres.2015.11.004.

Eldeberky, Y., Battjes, J.A., 1996. Spectral modeling of wave breaking: application to Boussinesq equations. J. Geophys. Res. 101 (C1), 1253–1264, http://dx.doi.org/10.1029/95JC03219.

Elfrink, B., Brøker, I., Deigaard, R., Hansen, E.A., Justesen, P., 1996. Modelling of 3D sediment transport in the surf zone. In: Proceedings of the 25th International Conference on Coastal Engineering, ASCE, Orlando, FL, USA, 3805–3817.

Engelund, F., Fredsøe, J., 1976. A sediment transport model for straight alluvial channels. Hydrol. Res. 7 (5), 293–306.

Ferreira, Ó., 2005. Storm groups versus extreme single storms: predicted erosion and management consequences. J. Coastal Res. 42, 221–227.

Foteinis, S., 2014. Erosion of coastlines of Greece: assessment – responses. (Ph.D. thesis). Tech. Univ. Crete, School of Environmental Engineering (in Greek).

Fredsøe, J., 1984. Turbulent boundary layers in wave-current motion. J. Hydraul. Eng.-ASCE 110 (8), 1103–1120, http://dx.doi.org/10.1061/(ASCE)0733-9429(1984)110:8(1103).

Gong, Z., Zhang, C.-K., Zuo, C.-B., Wu, W.-D., 2011. Sediment transport following water transfer from Yangtze River to Taihu Basin. Water Sci. Eng. 4 (4), 431–444, http://dx.doi.org/10.3882/j.issn.1674-2370.2011.04.007.

Hanson, H., Aarninkhof, S., Capobianco, M., Jimenez, J.A., Larson, M., Nicholls, R.J., Plant, N.G., Southgate, H.N., Steetzel, H.J., Stive, M.J.F., de Vriend, H.J., 2003. Modelling of coastal evolution on yearly to decadal time scales. J. Coastal Res. 19 (4), 790–811.

Hasselmann, K., 1974. On the spectral dissipation of ocean waves due to whitecapping. Bound.-Layer Meteorol. 6 (1), 107–127.

Hasselmann, S., Hasselmann, K., Allender, J.H., Barnett, T.P., 1985. Computations and parameterizations of the nonlinear energy transfer in a gravity wave spectrum. Part II: Parameterizations of the nonlinear energy transfer for application in wave models. J. Phys. Oceanogr. 15, 1378–1391, http://dx.doi.org/10.1175/1520-0485(1985)015<1378:CAPOTN>2.0.CO;2.

Ikeda, S., Osawa, K., Akamatsu, Y., 2009. Sediment and nutrients transport in watershed and their impact on coastal environment. Proc. Jpn. Acad. Ser. B: Phys. Biol. Sci. 85 (9), 374–390, http://dx.doi.org/10.2183/pjab.85.374.

Janssen, P.A.E.M., 1989. Wave-induced stress and the drag of air flow over sea waves. J. Phys. Oceanogr. 19, 745–754, http://dx.doi.org/10.1175/1520-0485(1989)019<0745:WISATD>2.0.CO;2.

Janssen, P.A.E.M., 1991. Quasi-linear theory of wind wave generation applied to wave forecasting. J. Phys. Oceanogr. 21, 1631–1642, http://dx.doi.org/10.1175/1520-0485(1991)021<1631:QLTOWW>2.0.CO;2.

Janssen, P.A.E.M., 1992. Consequences of the effect of surface gravity waves on the mean air flow. In: Banner, M.L., Grimshaw, R.H.J. (Eds.), Breaking Waves, International Union of Theoretical And Applied Mechanics (IUTAM) Symposium Sydney, Australia.

Janssen, P.A.E.M., Lionello, P., Zambresky, L., 1989. On the interaction of wind and waves. Phil. Trans. R. Soc. A 329 (1604), 289–301, http://dx.doi.org/10.1098/rsta.1989.0077.

Jara, M.S., González, M., Medina, R., 2015. Shoreline evolution model from a dynamic equilibrium beach profile. Coast. Eng. 99, 1–14, http://dx.doi.org/10.1016/j.coastaleng.2015.02.006.

Jing-Jing, X., Fei, H., Zi-Niu, X., Xue-Ling, C., 2014. Bias correction in wind direction forecasting using the circular-circular regression method. Atmos. Oceanic Sci. Lett. 7 (2), 87–91, http://dx.doi.org/10.3878/j.issn.1674-2834.13.0057.

Johnson, H.K., Kofoed-Hansen, H., 2000. Influence of bottom friction on sea surface roughness and its impact on shallow water wind wave modelling. J. Phys. Oceanogr. 30, 1743–1756, http://dx.doi.org/10.1175/1520-0485(2000)030<1743:IOBFOS>2.0.CO;2.

Karathanasi, F.E., Soukissian, T.H., Axaopoulos, P.G., 2016. Calibration of wind directions in the Mediterranean Sea. In: Proceedings of the 26th International Ocean and Polar Engineering Conference (ISOPE) 1, Rhodes, Greece, 491–497.

Karunarathna, H., Horrillo-Caraballo, J.M., Reeve, D.E., 2012. Prediction of cross-shore beach profile evolution using a diffusion type model. Cont. Shelf Res. 48, 157–166, http://dx.doi.org/10.1016/j.csr.2012.08.004.

Karunarathna, H., Pender, D., Ranasinghe, R., Short, A.D., Reeve, D.E., 2014. The effects of storm clustering on beach profile variability. Mar. Geol. 348, 103–112, http://dx.doi.org/10.1016/j.margeo.2013.12.007.

Komen, G.J., Cavaleri, L., Doneland, M., Hasselmann, K., Hasselmann, S., Janssen, P.A.E.M., 1994. Dynamics and Modeling of Ocean Waves, Cambridge Univ. Press, UK, 532 pp., http://dx.doi.org/10.1017/S0022112096220166.

Kontoyiannis, H., 2010. Observations on the circulation of the Saronic Gulf: a Mediterranean embayment sea border of Athens, Greece. J. Geophys. Res. 115 (C6), 2156–2202, http://dx.doi.org/10.1029/2008JC005026.

Larroudé, P., 2008. Methodology of seasonal morphological modelisation for nourishment strategies on a Mediterranean beach. Mar. Pollut. Bull. 57 (1–5), 47–52, http://dx.doi.org/10.1016/j.marpolbul.2008.04.039.

Lesser, G.R., Roelvink, J.A., van Kester, J.A.T.M., Stelling, G.S., 2004. Development and validation of a three-dimensional morphological model. Coast. Eng. 51 (8–9), 883–915, http://dx.doi.org/10.1016/j.coastaleng.2004.07.014.

Li, M., Fernando, P.T., Pan, S., O'Connor, B.A., Daoyi Chen, D., 2007. Development of a quasi-3d numerical model for sediment transport prediction in the coastal region. J. Hydro-Environ. Res. 1 (2), 143–156, http://dx.doi.org/10.1016/j.jher.2007.09.001.

Luo, S., Liu, Y., Jin, R., Zhang, J., Wei, W., 2016. A guide to coastal management: benefits and lessons learned of beach nourishment practices in China over the past two decades. Ocean Coast. Manage. 134, 207–215, http://dx.doi.org/10.1016/j.ocecoaman.2016.10.011.

Masselink, G., Short, A.D., 1993. The effect of tide range on beach morphodynamics and morphology: a conceptual beach model. J. Coastal Res. 9 (3), 785–800.

Mayerle, R., Narayanan, R., Etri, T., Wahab, A.K.A., 2015. A case study of sediment transport in the Paranagua Estuary Complex in Brazil. Ocean Eng. 106, 161–174, http://dx.doi.org/10.1016/j.oceaneng.2015.06.025.

Nam, P.T., Larson, M., Hanson, H., Hoan, L.X., 2009. A numerical model of nearshore waves, currents, and sediment transport. Coast. Eng. 56 (11–12), 1084–1096, http://dx.doi.org/10.1016/j.coastaleng.2009.06.007.

Neumann, B., Vafeidis, A.T., Zimmermann, J., Nicholls, R.J., 2015. Future coastal population growth and exposure to sea-level rise and coastal flooding — a global assessment. PLoS ONE 10 (6), e0131375, http://dx.doi.org/10.1371/journal.pone.0118571.

Papadopoulos, A., Katsafados, P., Mavromatidis, E., Kallos, G., 2008. Assessing the skill of the POSEIDON-II weather forecasting system, Abstracts Books of the EuroGOOS 2008 Conference.

Papanicolaou, A.N., Elhakeem, M., Krallis, G., Prakash, S., Edinger, J., 2008. Sediment transport modeling review — current and future developments. J. Hydraul. Eng.-ASCE 134, 1—14, http://dx.doi.org/10.1061/(ASCE)0733-9429(2008)134:1(1).

Poorhosein, M., Afzalimehr, H., Sui, J., Singh, V.P., Azareh, S., 2014. Empirical bed load transport equations. Int. J. Hydraul. Eng. 3 (3), 93—101.

Requejo, S., Medina, R., González, M., 2008. Development of a medium—long term beach evolution model. Coast. Eng. 55 (12), 1074—1088, http://dx.doi.org/10.1016/j.coastaleng.2008.04.005.

Ruessink, B.G., Terwindt, J.H.J., 2000. The behaviour of nearshore bars on the time scale of years: a conceptual model. Mar. Geol. 163 (1—4), 289—302, http://dx.doi.org/10.1016/S0025-3227(99)00094-8.

Samaras, A.G., Gaeta, M.G., Miquel, A.M., Archetti, R., 2016. High-resolution wave and hydrodynamics modelling in coastal areas: operational applications for coastal planning, decision support and assessment. Nat. Hazards Earth Syst. Sci. 16 (6), 1499—1518, http://dx.doi.org/10.5194/nhess-16-1499-2016.

Samaras, A.G., Koutitas, C.G., 2014. Comparison of three longshore sediment transport rate formulae in shoreline evolution modeling near stream mouths. Ocean Eng. 92, 255—266, http://dx.doi.org/10.1016/j.oceaneng.2014.10.005.

Shengcheng, J.I., Ouahsine, A., Smaoui, H., Sergent, P., 2014. 3D modeling of sediment movement by ships-generated wakes in confined shipping channel. Int. J. Sediment Res. 29 (1), 49—58, http://dx.doi.org/10.1016/S1001-6279(14)60021-4.

Simons, R.K., Canali, G.E., Anderson-Newton, G.T., Cotton, G.K., 2000. Sediment transport modeling: calibration, verification, and evaluation. J. Soil Contam. 9 (3), 261—289.

Skanavis, V., 2013. Geological and anthropogenic factors in the formation of coastline: the case study of Varkiza — S. Attica. (Diploma Thesis). Tech. Univ. Crete, School of Mineral Resources Engineering (in Greek).

Soukissian, T.H., Chronis, G., Nittis, K., 1999. POSEIDON: operational marine monitoring system for Greek seas. Sea Technol. 40 (7), 31—37.

Sulis, A., Annis, A., 2014. Morphological response of a sandy shoreline to a natural obstacle at Sa Mesa Longa Beach, Italy. Coast. Eng. 84, 10—22, http://dx.doi.org/10.1016/j.coastaleng.2013.10.014.

Trucano, T.G., Swiler, L.P., Igusa, T., Oberkampf, W.L., Pilch, M., 2006. Calibration, validation, and sensitivity analysis: what's what. Reliab. Eng. Syst. Safe. 91 (10—11), 1331—1357, http://dx.doi.org/10.1016/j.ress.2005.11.031.

Van Rijn, L.C., Ribberink, J.S., Van Der Werf, J., Walstra, D.J.R., 2013. Coastal sediment dynamics: recent advances and future research needs. J. Hydraul. Res. 51 (5), 475—493, http://dx.doi.org/10.1080/00221686.2013.849297.

Weitz, J., Demlie, M., 2014. Conceptual modelling of groundwater—surface water interactions in the Lake Sibayi Catchment, Eastern South Africa. J. Afr. Earth Sci. 99 (Pt. II), 613—624, http://dx.doi.org/10.1016/j.jafrearsci.2013.11.018.